JOURNAL OF THERMOPHYSICS AND HEAT TRANSFER
Vol. 24, No. 2, April–June 2010

Encapsulated Phase Change Material Slurry Flow in Manifold Microchannels

Sarada Kuravi,* Jianhua Du,† and Louis C. Chow‡
University of Central Florida, Orlando, Florida 32816-2450

DOI: 10.2514/1.44276

The heat transfer performance of water-based microencapsulated phase change material slurry (particle size 5 μm) flow inside manifold microchannels of hydraulic diameter 170 μm was experimentally and numerically investigated. Slurry performance was poorer compared with pure fluid due to the large size of particles used and lower thermal conductivity of slurry compared with water. A parametric study was performed with nanoencapsulated phase change material slurry flow (particle size of 100 nm) in microchannels of hydraulic diameters 170 and 47 μm. Two different base fluids were considered and the heat transfer enhancement of slurry with various particle mass concentrations compared with its base fluid was presented. For developing flows, the performance of phase change material slurry depends on various parameters such as base-fluid thermal conductivity, channel dimensions, amount of phase change material melted, and particle mass concentration. In the case of manifold microchannel heat sinks, where the microchannel flowpath is much shorter compared with traditional microchannels, using higher-thermal-conductivity phase change material, narrower channels, smaller particles, and optimum parameters will aid in obtaining better thermal performance of phase change material slurry compared with pure fluid.

Nomenclature

A_b = area of base, m^2
Bi_p = Biot number of particle
c = volume concentration of microencapsulated phase change material particles in slurry
c_m = mass concentration of microencapsulated phase change material particles in slurry
$c_{p,b}$ = specific heat of bulk fluid, $J/kg \cdot K$
$c_{p,f}$ = specific heat of fluid, $J/kg \cdot K$
$c_{p,p}$ = specific heat of microencapsulated phase change material particle, $J/kg \cdot K$
$c_{p,\mathrm{pcm}}$ = specific heat of phase change material $J/kg \cdot K$
d_p = particle diameter, m
e = magnitude of shear rate, $1/s$
f = enhancement factor
H = height of the channel, m
H_m = height of manifold in simulation domain, m
h = heat transfer coefficient, $W/m^2 \cdot K$
h_r = heat transfer coefficient ratio, $h_{\mathrm{slurry}}/h_{\mathrm{base\ fluid}}$
h_{sf} = latent heat of fusion, J/kg
k = thermal conductivity, $W/m \cdot K$
k_b = thermal conductivity of bulk fluid, $W/m \cdot K$
k_{eff} = effective thermal conductivity of bulk fluid, $W/m \cdot K$
k_f = thermal conductivity of fluid, $W/m \cdot K$
k_p = thermal conductivity of microencapsulated phase change material particle, $W/m \cdot K$
k_{pcm} = thermal conductivity of phase change material, $W/m \cdot K$
L = length of the channel, m
L_m = half of manifold length in simulation domain, m
Pe = Peclet number
PF = $\Delta P_{\mathrm{base\ fluid}}/\Delta P_{\mathrm{slurry}}$, when $h_{\mathrm{slurry}} = h_{\mathrm{base\ fluid}}$
p = pressure, psi
p_{in} = pressure at the inlet, psi
p_{out} = pressure at the outlet, psi
Q = heat supplied, W
q = heat flux, W/cm^2
q_w = constant wall heat flux, W/cm^2
R_p = radius of microencapsulated phase change material particle, m
r_p = solid liquid interface radius, m
T = temperature, K
T_{in} = temperature at heat-sink inlet and at microchannel inlet, K
T_m = melting temperature, K
T_{mr} = melting range, $T_1 - T_2$, K
T_{out} = temperature at heat-sink outlet and at microchannel outlet, K
T_w = wall temperature, K
$T_{w,\max}$ = maximum wall temperature, K
T_1 = lower melting temperature, K
T_2 = higher melting temperature, K
t_{base} = base of microchannel, m
t_{ch} = half of microchannel width, m
t_{res} = residence time of microencapsulated phase change material particle inside the channel, s
t_w = half of microchannel wall thickness, m
$\boldsymbol{u}$ = velocity vector
u = velocity in x direction, m/s
V_{HS} = volumetric flow rate at the heat-sink inlet, m^3/s
$\mathbf{v}$ = velocity vector
v = velocity in y direction, m/s
w = velocity in z direction, m/s
x, y, z = spatial coordinates
$\mathbf{x}$ = space vector
α_f = thermal diffusivity of fluid, m^2/s
α_p = thermal diffusivity of microencapsulated phase change material particle, m^2/s
γ = shear rate, $1/s$
ΔP = pressure drop, psi
ΔP_r = pressure drop ratio, $\Delta P_{\mathrm{slurry}}/\Delta P_{\mathrm{base\ fluid}}$
ΔT_{bulk} = bulk temperature rise, $T_{\mathrm{out}} - T_{\mathrm{in}}$, K

Presented as Paper 4097 at the 41st Thermophysics Conference, San Antonio, TX, 22–25 June 2009; received 10 March 2009; revision received 26 October 2009; accepted for publication 19 November 2009.

*Ph.D. Student, Department of Mechanical, Materials and Aerospace Engineering. Student Member AIAA.
†Research Professor, Department of Mechanical, Materials and Aerospace Engineering.
‡Professor and University Chair, Department of Mechanical, Materials and Aerospace Engineering, Associate Fellow AIAA.

μ = dynamic viscosity, Pa · s
μ_b = dynamic viscosity of bulk fluid, Pa · s
μ_f = dynamic viscosity of fluid, Pa · s
μ_p = dynamic viscosity of microencapsulated phase change material particle, Pa · s
ρ = density, kg/m^3
ρ_b = density of bulk fluid, kg/m^3
ρ_f = density of fluid, kg/m^3
ρ_p = density of microencapsulated phase change material particle, kg/m^3

I. Introduction

THE use of encapsulated phase change slurry as heat transfer fluid is gaining more interest due to the capability of high convective heat transfer and thermal storage performance of slurry. As shown by several researchers, both experimentally and numerically [1–13], microencapsulated phase change material (MEPCM) slurries can enhance the heat transfer coefficient and considerably reduce the mass flow rate, wall temperature, and pumping power compared with single-phase fluids. Colvin and Mulligan [1,2] reported that with increase of specific heat of fluid by using phase change material (PCM) slurry, for the same temperature rise, the flow rate can be reduced to one-tenth (or by 90%) and the pumping power can be reduced to one-hundredth (or by 99%) for a given heat flux. Similar reductions in pumping power have also been reported by Goel et al. [6]. Theoretical analysis by Kasza and Chen [4] showed that heat transfer enhancement of threefold or higher can be achieved for certain heat transfer geometries by using PCM slurry compared with single-phase fluid.

It should be noted that these conclusions by several investigators were drawn for phase change slurry flows in conventional long channels in which the flows are fully developed. When the flow is not fully developed, thermal conductivity of the fluid also plays an important role in defining the performance of slurry [14,15]. This was observed in both laminar and turbulent flow through ducts. Rao et al. [14] performed comparative flow and heat transfer experiments in rectangular minichannels with water as the base fluid and *n*-octadecane as the phase change material. It was found that the performance of slurry is less effective at high mass flow rates and high mass concentrations. It was concluded that the low thermal conductivity of slurry compared with water and low residence time of particles with increase in mass flow rates were the reasons for the poor performance of slurry.

Few researchers have studied the PCM slurry flow in microchannels numerically [12,13,16,17]. Hao and Tao [12] and Xing et al. [13] have simulated the heat transfer performance in microtubes. They concluded that a low Reynolds number condition must be maintained in order to take full advantage of heat transfer enhancement in microchannel flow. Kuravi et al. [16] have studied the performance of nanoencapsulated phase change material (NEPCM) slurry flow in manifold microchannels with a base fluid that has thermal conductivity equal to that of PCM. They found that slurry performs better compared with pure single-phase fluid even in thermally developing flows. Sabbah et al. [17] studied the performance of water-based slurry in rectangular channels and concluded that heat transfer enhancement depends on the channel inlet and outlet temperatures and melting range of PCM.

In the current study, performance of encapsulated phase change material slurry in manifold microchannels is investigated and compared with that of single-phase fluid. Experiments performed until now with MEPCM slurries were in conventional channels or in minichannels, with the smallest channel hydraulic diameter being 2.71 mm. In the current study, experiments were performed in microchannels with a 170 μm hydraulic diameter as a first attempt to evaluate the performance of encapsulated phase change material slurry flow in microchannels. A numerical model presented in [16] was used to conduct the parametric study and focused on the effect of relative thermal conductivity between the base fluid and PCM, geometric features, and mass concentration in evaluating the slurry performance.

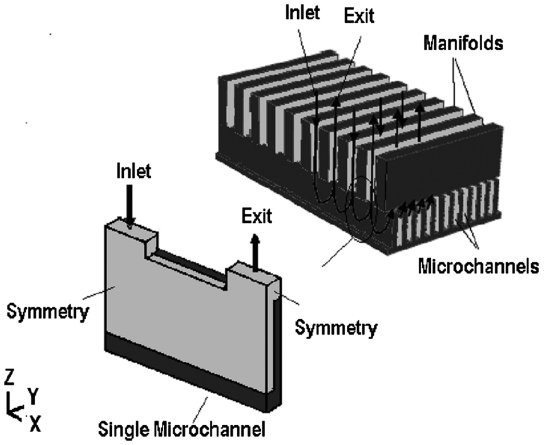

Fig. 1 MMC heat-sink flowpath and flow domain.

The MMC heat sink (Fig. 1 shows the geometry and flow domain inside a single microchannel) features many inlet and outlet channels alternating at a periodic distance (~1 mm) along the length of the MMC. The flow enters the microchannels from the manifold inlet channel, splits, and flows through the microchannels, then exits to the manifold outlet channel. This pattern is repeated along the length of the MMC. Because of the short length of the channel, the pressure drop in the case of MMC heat sinks is lower compared with traditional microchannels.

II. Experimental Investigation

Baseline experiments were performed in custom-fabricated microchannel heat sinks. These heat sinks were fabricated at Microcooling Concepts, Inc., with an average footprint of 1 × 2 cm and are similar to the conventional manifold microchannel heat sinks. For illustration purposes, Fig. 2 shows the possible fluid path and Fig. 3 shows the photograph of the fabricated part. There are approximately 441 microchannels inside the heat sink and each channel is approximately is 101 μm wide, 533 μm high, and 1 mm long.

As shown in Fig. 4, the MEPCM particle consists of phase change material enclosed in a thin polymer shell. MEPCM slurry made at BASF was used and consisted of particles of diameter of 5 μm mixed in water. The core material is *n*-octadecane and the shell material is polymethylmetacrylate (PMMA). The physical properties of the suspension and the suspension components used for experiment and numerical simulation are shown in Table 1.

The density of the bulk fluid is calculated as

$$\rho_b = c\rho_p + (1 - c)\rho_f \tag{1}$$

The particle density is calculated based on the densities of the PCM and shell material and their volume fractions, where the PCM average volume fraction in the particle is around 90%.

The effective specific heat of slurry is calculated as [10]

$$c_{p,b} = c_m c_{p,p} + (1 - c_m)c_{p,f} \tag{2}$$

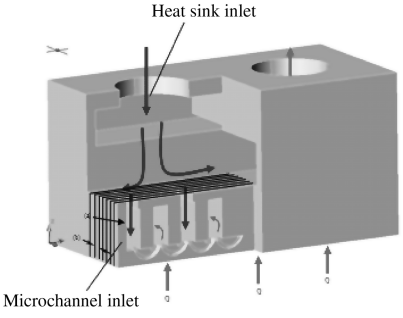

Fig. 2 Possible fluid path in the fabricated microchannels.

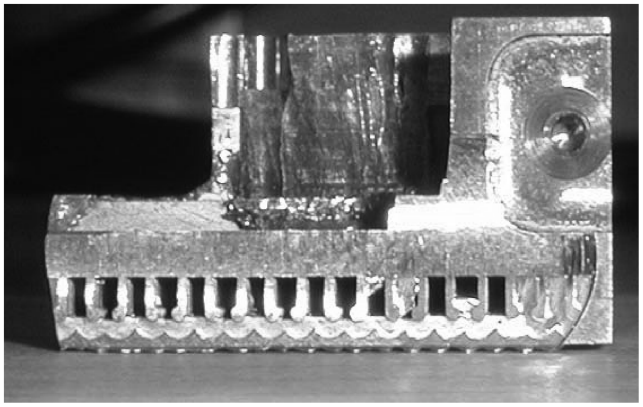

Fig. 3 Cross section of the fabricated heat sink.

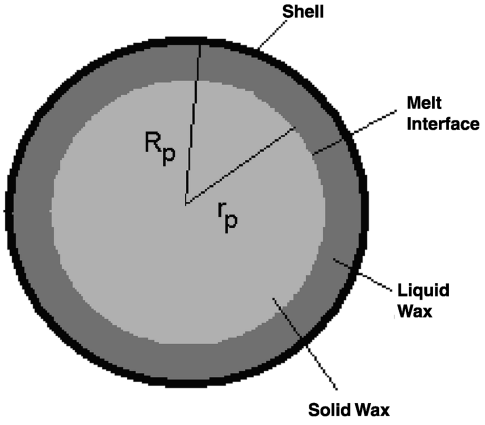

Fig. 4 Particle melting process.

The bulk thermal conductivity of the slurry suspension can be estimated by using the Maxwell correlation [7]:

$$k_b = k_f \cdot \frac{2 + \frac{k_p}{k_f} + 2c\left(\frac{k_p}{k_f} - 1\right)}{2 + \frac{k_p}{k_f} - c\left(\frac{k_p}{k_f} - 1\right)} \tag{3}$$

The slurry viscosity is usually calculated using Vand's correlation [18,19]:

$$\frac{\mu_b}{\mu_f} = (1 - c - 1.16c^2)^{-2.5} \tag{4}$$

In [14], similar particles were used and it was mentioned that the measured viscosity values deviates from Vand's correlation [18,19], which is usually used for calculating bulk viscosity. This equation is derived for spherical particles. In reality, as the particles are not spherical in nature, viscosity value predicted by this correlation may not be accurate. Hence, the measured/experimental value provided in [14] was used instead of Eq. (4) for calculating the bulk viscosity. The latent melting enthalpy of PCM was measured using differential scanning calorimetry (DSC) and was found to be 120 kJ/kg between 23 and 29°C.

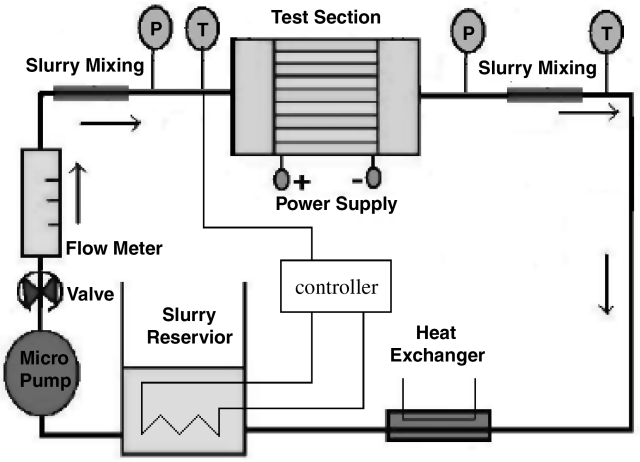

Fig. 5 Schematic of the experimental setup.

A. Experimental Setup

Figure 5 illustrates the schematic of the flow loop for the experiments. It consists of a microchannel heat exchanger, a pump, a valve, a flowmeter, two mixing sections at both the inlet and outlet of the heat exchanger, and a plate heat exchanger. The working fluid was pumped from the fluid reservoir using a diaphragm pump. The valve was used for flow rate adjustment in the loop. The flow rate was measured using two Coriolis flow meters with a scale of 20 gal/h (21.03×10^{-6} m^3/s) and 40 gal/h (42.06×10^{-6} m^3/s) (one is for small flow rate and one is for large flow rate). The two mixing sections were used to mix fluid thoroughly so that the thermocouples measure the bulk temperature at the inlet and outlet of the heat exchanger. The plate heat exchanger was used to cool down working fluid after it leaves the test section. The temperature was set to below resolidifying temperature of the PCM material. The heater in the reservoir was used to adjust the fluid temperature at the inlet of the microchannel heat exchanger. Two thin-film resistors soldered at the bottom of the microchannel heat exchanger were used as heating source in the experiments. Power to the resistors was supplied by an adjustable dc power supply to vary the amount of heat generated by the heater. Two thermocouples were attached to the back of the thin-film resistors to measure the heater temperature. Power to the heater was calculated by measuring the voltage across the heater and the current that passes through the heater. The resistors were thermally insulated in the experiments. Since most of the heat that is generated by the heater will be absorbed by the microchannel heat exchanger, it was assumed that the measured temperature at the heater is equal to the wall temperature of the heat exchanger. The temperature at the outlet of the plate exchanger was monitored so that working fluid is cooled below the resolidifying temperature during the tests on slurry.

B. Experimental Results

Experiments were performed with pure water and slurry with mass concentration 0.1 (to avoid clogging). Figure 6 shows the pressure drop obtained across the heat sink at different inlet flow rates. The pressure drop of slurry is higher compared with water for all the flow rates, due to the increase in viscosity of the fluid. Tables 2 and 3 show the experiment conditions and heat transfer results obtained with water and slurry. Figure 7 shows the heat transfer coefficient of water and slurry at different flow rates. The heat transfer performance was evaluated by comparing the heat transfer coefficient defined as

Table 1 Properties of the suspension components used for experiments [14]

	Density, kg/m^3	Specific heat, J/kg · K	Thermal conductivity, W/m · K	Viscosity, kg/m · s	Latent heat kJ/kg
Water	997	4180	0.604	1×10^{-3}	——
MEPCM particle	867	1900	0.164	——	120
Slurry (10%)	982	3950	0.541	2.3×10^{-3}	——

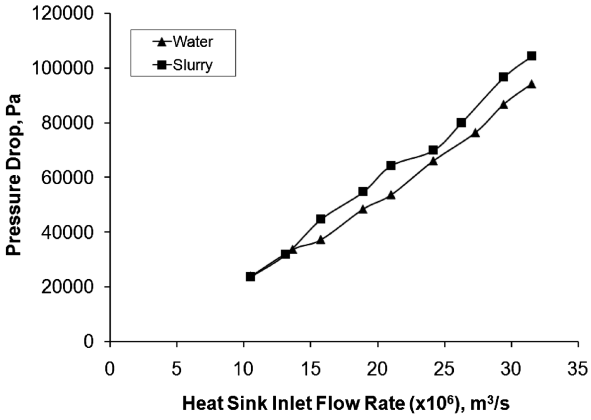

Fig. 6 Experimental results: pressure drop.

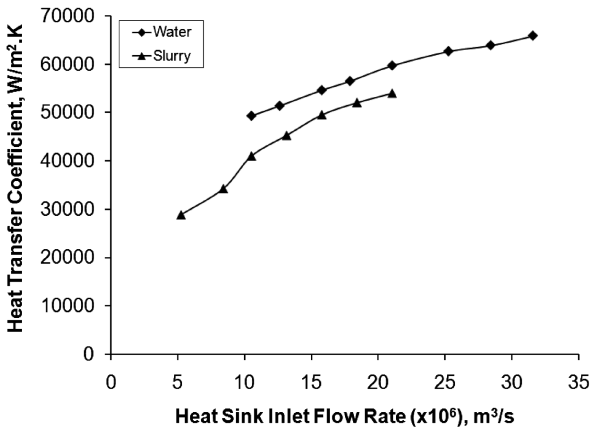

Fig. 7 Heat transfer coefficient of water and slurry.

$$h = \frac{Q}{A_b(T_w - T_{\text{in}})} \tag{5}$$

where T_w is the wall temperature at the heater. It can be seen that heat transfer coefficient of slurry is lower than heat transfer coefficient of water (base fluid). The error in power calculation from the voltage and current measurement can be ignored in the experiments. The error in flow rate measurements was estimated to be less than 5%. The error in temperature measurement is within 0.2°C. Thermal balance between supplied power to the heater and amount absorbed by working fluid in the water experiments was less than 6.3%. The error in heat transfer coefficient calculated based on the measurement was estimated to be less than 8%.

C. Analysis of Experimental Results

The performance of slurry is poorer compared with pure water at all the flow rates. The possible reasons for this behavior of slurry could be due to the following.

1. Low Thermal Conductivity of Slurry Compared with Water

The presence of PCM particles increases the heat capacity of the fluid (during melting), but also decreases the effective thermal conductivity and sensible heat capacity. In the case of fully developed flows, high specific heat fluid always performed better, as shown by many researchers. This is because the heat has already reached the center of the channel and the effect of high specific capacity of the fluid dominates the effect of lowering of thermal conductivity, due to the presence of PCM. When the flow is not thermally fully developed, the heat transfer performance of slurry depends on how effectively the heat is transferred to the fluid. Low thermal conductivity results in less heat transfer to the fluid.

Table 2 Heat transfer results (with water)

V_{HS} ($\times 10^{-6}$, m^3/s)	Q, W	T_{in}, °C	T_{out}, °C	T_w, °C
10.51	360	33.8	42.0	70.3
12.62	360	35.2	42.3	70.3
15.77	360	34.2	40.0	67.2
17.87	360	34.4	39.4	66.3
21.03	361	33.1	37.1	63.3
25.24	360	37.0	40.2	65.7
28.39	360	35.6	38.5	63.8
31.54	361	33.2	35.9	60.6

Table 3 Heat transfer results (with slurry)

V_{HS} ($\times 10^{-6}$, m^3/s)	Q, W	T_{in}, °C	T_{out}, °C	T_w, °C
5.26	184	22.1	32.8	53.9
8.41	184	24.6	31.5	51.4
10.51	360	23.6	32.6	67.5
13.14	360	24.9	32.0	64.7
15.77	360	25.2	30.7	61.6
18.40	360	24.9	29.4	59.5
21.03	361	24.8	28.6	58.2

2. Little or No Melting of PCM Particles Inside the Channel

Since the length of the channel is short for the MMC channel, it is important that the PCM particle completely melts within its residence time. Charunyakorn et al. [7] applied the method proposed by Tao [20] to calculate solid–liquid or melt interface r_p (Fig. 4) in a sphere for calculating the source term in their model. Assuming the particle has to melt 99% by the time it exits the channel, the required temperature difference between the surrounding fluid T_f and the melting temperature T_m of the PCM was calculated in Eq. (6) using the same analogy:

$$T_{fm} = T_f - T_m = \left[\frac{1}{2}\left[1 - \left(\frac{r_p}{R_p}\right)^2\right] + \frac{1}{3}\left[1 - \left(\frac{r_p}{R_p}\right)^3\right]\left(\frac{1}{Bi_p} - 1\right)\right] . \frac{h_{\text{sf}} . R_p^2}{t_{\text{res}} . \alpha_p . c_{p,p}} \tag{6}$$

where the Biot number of the particle is given by

$$Bi_p = \frac{k_{\text{eff}}}{k_{\text{pcm}}} \cdot \frac{2(1-c)}{2 - 3c^{\frac{1}{3}} + c} \tag{7}$$

Figure 8 shows the required temperature difference between the fluid and the particle melting temperature for a 5-μm-diam particle at different velocities. A velocity of 0.25 m/s corresponds to $V_{\text{HS}} = 5.26 \times 10^{-6}$ m^3/s, the lowest flow rate used in the experiments. Since the flow is not fully developed thermally, it is highly possible that a large portion of the fluid remained at the inlet temperature and this required temperature difference could not be achieved for all the particles inside the channel. Thus, within the short duration, it is

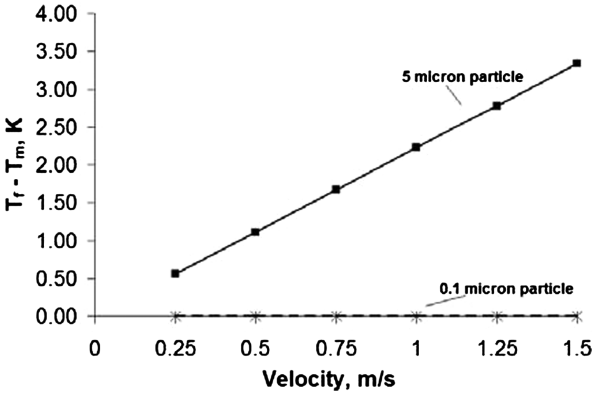

Fig. 8 Required temperature difference between particle surface and PCM melting temperature.

possible that most of the MEPCM particles have not melted or that only the particles near the wall might have partly melted.

III. Numerical Investigation

The schematic of the flow domain used is shown in Fig. 9. The walls represent microchannel walls and the fluid enters into the channel from the inlet and leaves from the exit. The inlet and outlet are separated by the dividers or manifolds (as shown in Fig. 1) and are not part of the simulation domain. Only half of the channel was considered for simulation because of symmetry. Configuration I of Table 4 is used for numerical simulation. The particle diameter used is 5 μm. From previous discussion, it is justifiable to assume that no PCM has melted in the experiments. Hence, the simulations were run assuming the bulk properties of slurry, as shown in Table 1. Copper is used as the wall material.

A. Numerical Model

1. Assumptions

1) Flow is steady and laminar.

2) The fluid can be considered as Newtonian for the particle concentration of 0.1 used in experiments [8].

3). The particle distribution is homogeneous so that the bulk properties are assumed constant [21].

4). The particles are assumed to follow the fluid without any lag, i.e., the difference in the particle and fluid velocities is negligible [16].

2. Governing Equations

The mass and momentum equations for the fluid inside the simulation domain can be written as

$$\frac{\partial u}{\partial x}+\frac{\partial v}{\partial y}+\frac{\partial w}{\partial z}=0 \tag{8}$$

$$\rho\left(u\frac{\partial u}{\partial x}+v\frac{\partial u}{\partial y}+w\frac{\partial u}{\partial z}\right)=-\frac{\partial p}{\partial x}+\mu\frac{\partial^2 u}{\partial x^2}+\mu\frac{\partial^2 u}{\partial y^2}+\mu\frac{\partial^2 u}{\partial z^2} \tag{9}$$

$$\rho\left(u\frac{\partial v}{\partial x}+v\frac{\partial v}{\partial y}+w\frac{\partial v}{\partial z}\right)=-\frac{\partial p}{\partial y}+\mu\frac{\partial^2 v}{\partial x^2}+\mu\frac{\partial^2 v}{\partial y^2}+\mu\frac{\partial^2 v}{\partial z^2} \tag{10}$$

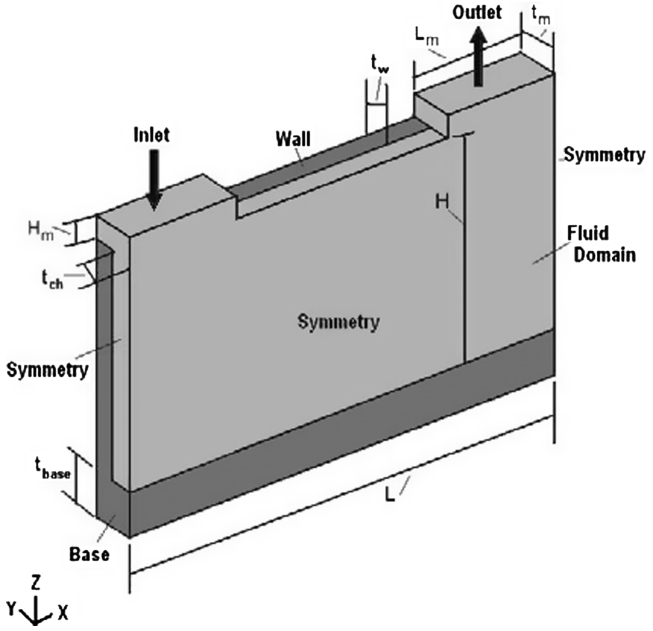

Fig. 9 Schematic of flow domain (not to scale).

Table 4 Geometric configurations used for numerical simulation (units in microns)

Configuration	H	2^*t_{ch}	L	H_m	L_m	2^*t_w	t_{base}
I	533	101	1000	50	250	352.52	250
II	375	25	1000	100	250	75	250

$$\rho\left(u\frac{\partial w}{\partial x}+v\frac{\partial w}{\partial y}+w\frac{\partial w}{\partial z}\right)=-\frac{\partial p}{\partial z}+\mu\frac{\partial^2 w}{\partial x^2}+\mu\frac{\partial^2 w}{\partial y^2}+\mu\frac{\partial^2 w}{\partial z^2} \tag{11}$$

The energy equation for the slurry is

$$\rho c_p\left(u\frac{\partial T}{\partial x}+v\frac{\partial T}{\partial y}+w\frac{\partial T}{\partial z}\right)=\frac{\partial}{\partial x}\left(k\frac{\partial T}{\partial x}\right)+\frac{\partial}{\partial y}\left(k\frac{\partial T}{\partial y}\right)+\frac{\partial}{\partial z}\left(k\frac{\partial T}{\partial z}\right) \tag{12}$$

The energy equation for the microchannel wall/fin is

$$\frac{\partial^2 T_w}{\partial x^2}+\frac{\partial^2 T_w}{\partial y^2}+\frac{\partial^2 T_w}{\partial z^2}=0 \tag{13}$$

3. Boundary Conditions

The boundary conditions for the flow inside the channels are as follows: no slip at the microchannel and manifold walls,

$$u=0 \tag{14}$$

atmospheric pressure at the microchannel outlet,

$$p=p_0 \tag{15}$$

and constant velocity at the inlet,

$$u=(0,0,|w|) \tag{16}$$

The boundary conditions for the heat transfer equations are as follows: constant heat flux at the base of the microchannel fin,

$$q\cdot n=q_w \tag{17}$$

adiabatic condition at all other outer walls,

$$q\cdot n=0 \tag{18}$$

constant inlet temperature at the manifold inlet,

$$T=T_{\text{in}} \tag{19}$$

convective heat flux boundary condition at the outlet/exit,

$$q\cdot n=(\rho c_p uT)\cdot n \tag{20}$$

continuity of temperature and heat flux at the wall and liquid interface,

$$T_w=T \tag{21}$$

$$-k_w\frac{\partial T_w}{\partial n}=-k_f\frac{\partial T_f}{\partial n} \tag{22}$$

4. Bulk Properties of Slurry

The bulk thermal conductivity of the slurry suspension can be defined as Eq. (3). The effective thermal conductivity of slurries in flow is enhanced due to the particle motions and particle–fluid interactions. It can be evaluated as follows [10]:

$$k_{\text{eff}} = f \cdot k_b \qquad \begin{cases} f = 1 + BcPe_p^m \\ B = 0, \quad m = 1.5, \quad Pe_p < 0.67 \\ B = 1.8, \quad m = 0.18, \quad 0.67 \le Pe_p \le 250 \\ B = 3.0, \quad m = \frac{1}{11}, \quad Pe_p > 250 \end{cases} \tag{23}$$

where the particle Peclet number is defined as

$$Pe_p = \frac{ed_p^2}{\alpha_f} \tag{24}$$

Since the velocity is not fully developed in the current analysis, the shear rate is a function of all the spatial coordinates and corresponding velocities. The magnitude of the shear rate e can be calculated using the following equation:

$$e = \left(\frac{1}{2}\sum_i \sum_j \gamma_{ij}\gamma_{ji}\right)^{1/2} \tag{25}$$

where γ is the shear rate. All other properties are used from Table 1.

B. Comparison of Experimental and Numerical Results

For comparing the numerical and experimental results, the particle size used is 5 μm and properties in Table 1 are used. Commercial finite element method software COMSOL® [22] was used for solving the flow and temperature fields. Configuration I of Table 4 and properties provided in Table 1 were used. The flow rate at the microchannel inlet was calculated based on the number of channels and total flow rate at the inlet of the heat sink. The wall thickness of the microchannel was used such that the base heat flux and the total heat supplied was the same as in experiments. In other words, twice the base area in the simulation domain multiplied by the number of channels is equal to the base area of the heat sink, which is 2 cm^2. Three different unstructured grid meshes consisting of elements 82,912, 143,580, and 295,667 were created using the default mesh option in COMSOL for checking the grid independency of results. The difference in results was not more than 0.15°C. Hence, the mesh consisting of 82,912 elements was used for all the runs in 101-μm-width channels. The pressure drop and bulk temperature rise obtained in both cases are presented in Table 5. The pressure drop and bulk temperature rise are defined as in Eq. (26), and the bulk mean temperature of the fluid at the exit is calculated as in Eq. (27):

$$\Delta P = p_{\text{in}} - p_{\text{out}} \qquad \Delta T = T_{\text{in}} - T_{\text{out}} \tag{26}$$

$$T_{\text{out}} = \frac{\int T c_{p,b}(n.\mathbf{u})\,\mathrm{d}s}{\int c_{p,b}(n.\mathbf{u})\,\mathrm{d}s} \tag{27}$$

where ds is the surface area at the outlet for Eq. (27).

Pressure drop predicted numerically ranges from 8.3 to 13.0% of total pressure drop obtained in experiments. This suggests that the pressure drop inside manifolds is higher compared with that of pressure drop inside the microchannels, which could be due to poor manifold design. Similar results were obtained in [23], in which the pressure drop in microchannels was 10% and the remaining 90% pressure drop in manifolds was attributed to the frictional losses, abrupt changes to the flow cross sections and the hard-edged flow directions. Proper design of the heat sink can result in more than 90% of pressure drop inside microchannels and less than 10% in manifolds, with the maximum theoretical microchannel pressure drop being 93% of total pressure drop [24]. Figure 10 shows the heat transfer coefficient obtained with numerical simulation and comparison with experimental results. The predicted maximum wall temperature using the numerical model does not account for the thermal resistance between the heater surface and the channel wall. Hence, the heat transfer coefficient obtained numerically is higher compared with experimental results.

Table 5 Numerical results obtained

Fluid	V_{HS} ($\times 10^{-6}$, m^3/s)	Q, W	T_{in}, °C	ΔT_{bulk}, °C	ΔP, Pa
Water	5.26	184	22.1	8.5	690
Water	10.51	360	33.8	8.2	2000
Water	15.77	360	34.2	5.8	4275
Slurry	5.26	184	22.1	8.9	1241
Slurry	10.51	360	23.6	8.7	3103
Slurry	15.77	361	25.2	6.1	5585

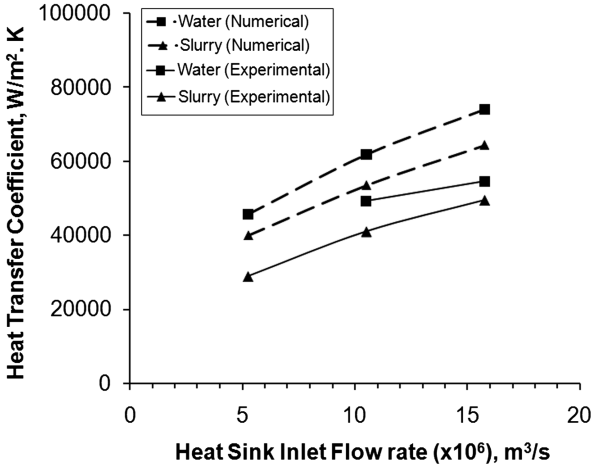

Fig. 10 Comparison of numerical and experimental results.

IV. Parametric Study

A parametric study was first done with two different base fluids in channels of 101 μm width, and a particle size of 100 nm was assumed. Smaller particles melt instantaneously, help in avoiding clogging, and can pass easily through narrow channels. NPCM also provide more heat transfer area to PCM because of higher surface-area-to-volume ratio compared with micron-sized PCM. Slurry was modeled as a bulk fluid with varying specific heat during the melting range. Properties of n-octadecane were used from [8], and the bulk properties are evaluated using Eqs. (1–4). Viscosity values based on Eq. (4) were used, as there are no available experimental values. The enhancement in thermal conductivity due to the presence of EPCM particles is neglected, since this value was found to be negligible for 100 nm particles [16]. A melting range of 10 K with peak melting point at 28°C (typical to n-octadecane) was used. For the grid independency check, meshes consisting of 68,285, 103,238, and 178,102 elements were used. The maximum difference in the results with these meshes was 0.12°C, and mesh consisting of 68,285 elements was used for all simulations.

A. Numerical Model for Parametric Study

1. Assumptions

A few more assumptions are used in the numerical model in order to account for the particle melting:

1) Flow is steady and laminar.

2) Particle concentrations used for the current study range from 0 to 0.3, and hence the fluid can be considered Newtonian [8].

3) The particle distribution is homogeneous so that the bulk properties are assumed constant except heat capacity, which is a function of temperature.

4) The melting inside MEPCM particles takes place over a range of temperatures between T_1 and T_2.

5) The particles are assumed to follow the fluid without any lag, i.e., the difference in the particle and fluid velocities is negligible [16].

6) There is no temperature gradient inside the particle or the particle melts instantaneously and there is no delay in absorption of heat inside the particle [16].

7) The effect of particle depletion layer is negligible [25,26].

8) As the shell that encapsulates the PCM is very thin in the case of 100 nm particle, its effect is neglected for the present simulation.

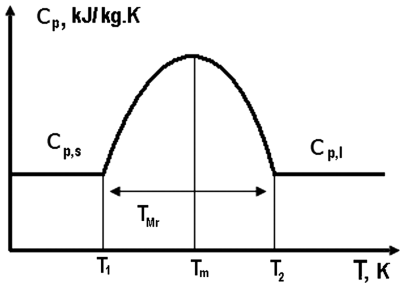

Fig. 11 Specific heat of encapsulated PCM as a function of temperature.

9) The shape of the encapsulated particles is spherical.

10) Brownian motion can be neglected for the high velocities used [27].

2. Effective Specific Heat

The sine profile shown in Fig. 11 has been used for the specific heat of the NEPCM particle and is described by Eq. (28). The specific heat of solid and liquid phases of PCM is assumed equal in the equation. This is justifiable, as there is not much variation in the property value:

$$c_{p,p} = c_{p,\text{pcm}} + \left\{\frac{\pi}{2}\cdot\left(\frac{h_{\text{sf}}}{T_{\text{mr}}} - c_{p,\text{pcm}}\right)\cdot \sin\pi\left[\frac{(T-T_1)}{T_{\text{mr}}}\right]\right\} \quad (28)$$

The maximum value of the specific heat during phase change is attained when the temperature of the slurry is in the melting range. The effective specific heat of the slurry can be calculated as shown in Eq. (2) [10].

The specific heat value of the particle is equal to $c_{p,\text{pcm}}$ when the temperature of the particle is outside the melting range and is given by Eq. (28) when the particle temperature is within the melting range.

B. Thermal Performance of Water and Polyalphaolefin-Based NEPCM Slurry in 101-μm-Wide Channels

The effect of base-fluid thermal conductivity was analyzed by using two different fluids: water and polyalphaolefin (PAO). PAO is a fluid used for avionics cooling and has thermal conductivity less than *n*-octadecane (Table 6). For comparison, a heat-sink inlet flow rate of 10.25×10^{-6} m^3/s and a heat flux of 180 W/cm^2 were used for both water- and PAO-based fluids. The inlet temperature used is 25°C, which is within the melting range. Configuration I (channel width 101 μm) of Table 4 was used. Figure 12 shows the bulk temperature rise predicted for both water and PAO. It can be observed that the bulk temperature rise decreases with increase in the particle mass concentration. Figure 13 shows the heat transfer coefficient ratio (h_r) of both water and PAO as the base fluid and is defined as

$$h_r = h_{\text{slurry}}/h_{\text{base fluid}} \quad (29)$$

In Fig. 13, $h_{\text{water}} = 61,832$ W/cm$^2\cdot$K and $h_{\text{PAO}} = 18,286$ W/cm$^2\cdot$K. The heat transfer coefficient decreases with increase in particle mass concentrations when water is used as the base fluid, except with mass concentration equal to 0.05. A slight increase in heat transfer coefficient at mass concentration of 0.05 indicates that the degradation in thermal conductivity is not significant, and hence the increase in the specific heat compared with base fluid helps the slurry performance. When PAO is used as the base fluid, the heat transfer coefficient increased with an increase in concentration. This shows that for developing PCM slurry flows, thermal conductivity plays a very important role in determining the slurry performance.

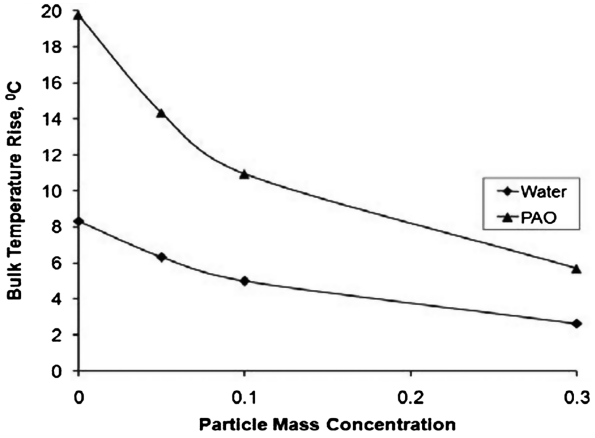

Fig. 12 Bulk temperature rise for water and PAO.

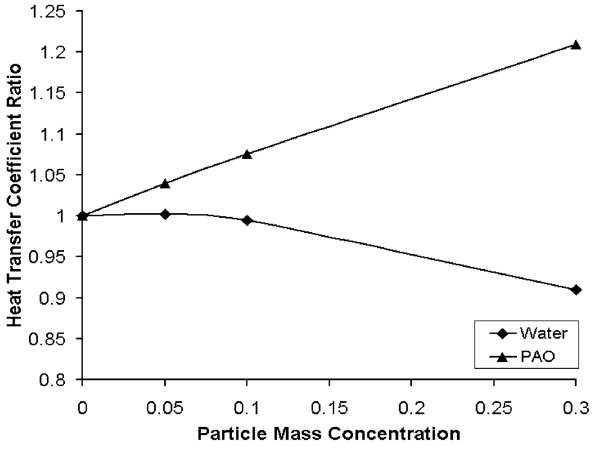

Fig. 13 Heat transfer coefficient ratio for water and PAO.

C. Thermal Performance of Water and PAO-Based NEPCM Slurry in 25-μm-Wide Channels

Figure 14 shows the temperature profile of water-based slurry in 101-μm-wide channels. From the figure, it can be observed that most of the fluid did not absorb heat, as the thermal boundary layer is not fully developed. To aid the thermal boundary in developing faster, numerical investigation was continued by using the simulation domain as configuration II (channel width 25 μm). The total number of channels inside the heat sink was 2000. An inlet flow rate of 10.51×10^{-6} m^3/s and heat flux of 180 W/cm^2 was used. Figure 15 shows the temperature profile of water-based slurry in 25-μm-wide channels. It can be observed that the temperature profile is more developed.

Figures 16 and 17 show the bulk temperature rise and heat transfer coefficient ratio predicted with water as the base fluid at different fluid inlet temperatures. The heat transfer coefficient of slurry is 1.5 times that of water at high mass concentration, enabling a maximum

Table 6 Thermophysical properties used for parametric study

	Density, kg/m^3	Specific heat, J/kg · K	Thermal conductivity, W/m · K	Viscosity, kg/m · s	Latent heat J/kg
PAO	783	2242	0.143	4.45×10^{-3}	——
n-octadecane	815	2000	0.18	——	244×10^3
Water	997	4180	0.604	1×10^{-3}	——
Copper	8700	385	400	——	——

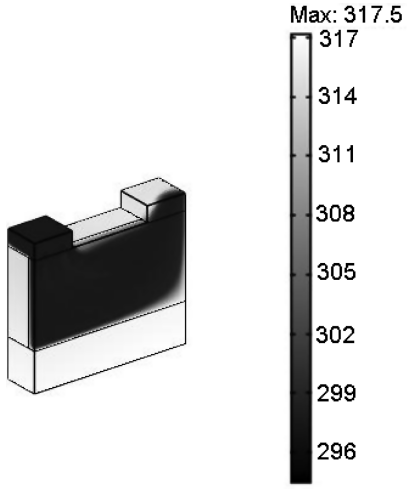

Fig. 14 Temperature profile of water-based slurry in 101-μm-wide channels (unit in Kelvin).

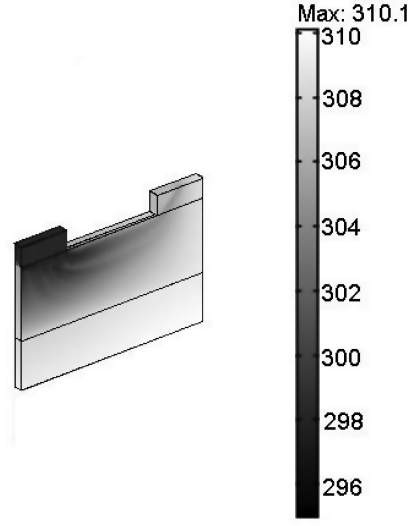

Fig. 15 Temperature profile of water-based slurry in 25-μm-wide channels (unit in Kelvin).

wall temperature decrease of 4 K. Figure 18 shows the bulk temperature rise obtained with PAO, as the base fluid and the heat transfer coefficient of PAO slurry (Fig. 19) is twice that of pure PAO at high concentration. The maximum wall temperature for 30% PAO slurry is 15 K lower than the maximum wall temperature of pure

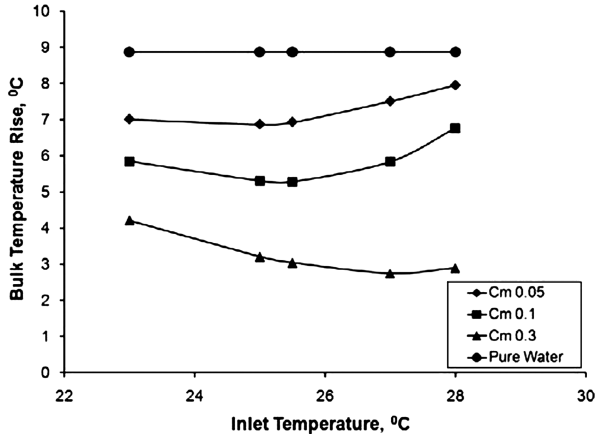

Fig. 16 Bulk temperature rise in the case of 25-μm-wide channels (base fluid–water).

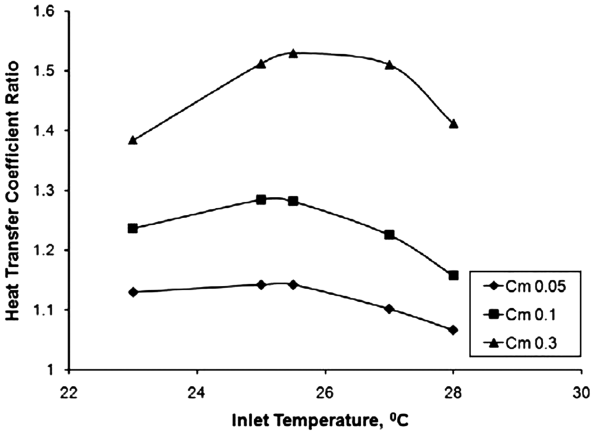

Fig. 17 Heat transfer coefficient ratio for water ($h_{\text{water}} = 150,695$ W/cm$^2 \cdot$ K).

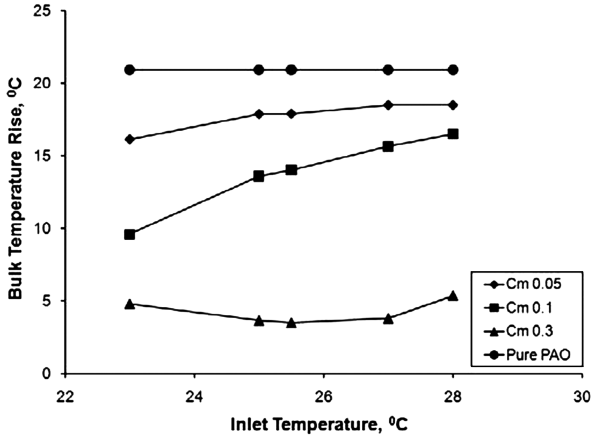

Fig. 18 Bulk temperature rise (base fluid–PAO).

PAO. Decreasing the channel width to 25 μm allows a higher number of fins within the heat sink. Compared with wider channels, a greater amount of fluid absorbs heat within each channel and the flow is closer to thermally fully developed, as the thermal entrance length is short in the case of narrow channels. Hence, using smaller-width channels enabling more heat transfer to the fluid helps to obtain better heat transfer coefficient for slurries, compared with pure base fluid. The amount of PCM that participates in heat absorption by the time the fluid exits the channel depends on the inlet temperature. For water, if the inlet temperature is around 25.5°C, the heat transfer coefficient is the highest, where as for PAO, it is 23°C.

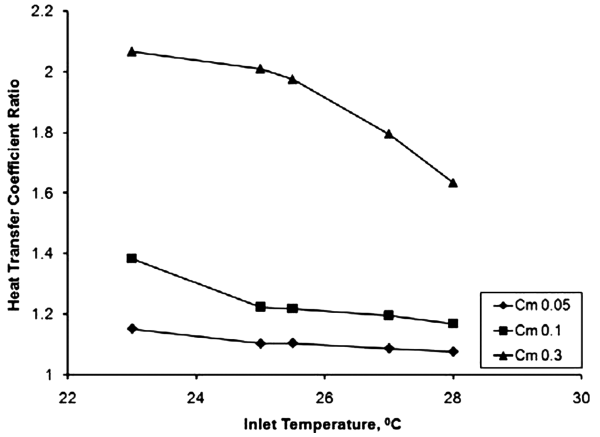

Fig. 19 Heat transfer coefficient ratio (base fluid–PAO, $h_{\text{PAO}} =$ 61,930 W/cm$^2 \cdot$ K.

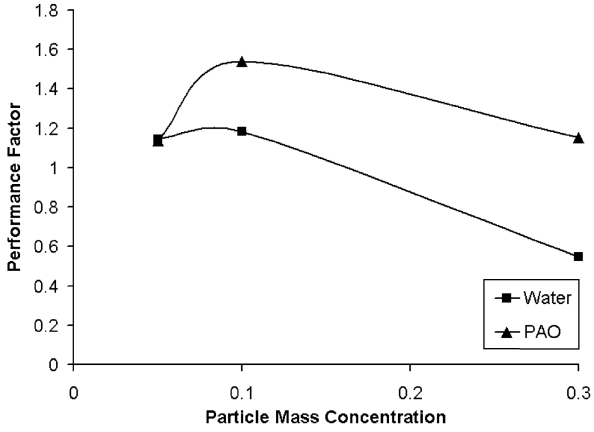

Fig. 20 Performance factor vs c_m.

D. Overall Performance of Water and PAO-Based Slurry in 25-μm-Wide Channels

To investigate the effect of high concentration on pressure drop, simulations were run using pure water and pure PAO to calculate performance factor PF, as defined in Eq. (30):

$$\mathrm{PF} = \Delta P_{\text{base fluid}} / \Delta P_{\text{slurry}} \tag{30}$$

This parameter signifies increase or decrease in the pressure drop when a pure fluid is used in order to achieve the heat transfer coefficient as slurry. For example, from Fig. 19, the heat transfer coefficient of water-based slurry at 5% concentration is $171,672\ \mathrm{W/cm^2 \cdot K}$ when the heat-sink inlet flow rate is $10.51 \times 10^{-6}\ \mathrm{m^3/s}$ and heat flux is $180\ \mathrm{W/cm^2}$. To achieve the same heat transfer coefficient with water, a higher heat-sink inlet flow rate was used and the resultant pressure drop inside the channel was 1.14 times of the pressure drop when 5% slurry was used. Figure 20 shows the PF with both water and PAO when the channel width is 25 μm and heat flux is $180\ \mathrm{W/cm^2}$. The heat-sink inlet flow rate used for pure water and PAO is higher than $10.51 \times 10^{-6}\ \mathrm{m^3/s}$ GPH, whereas for slurry it is $10.51 \times 10^{-6}\ \mathrm{m^3/s}$ for all the concentrations.

For high mass concentrations, the pressure drop in the case of slurry is higher compared with pure water for the same heat transfer coefficient. It can be concluded that particle mass concentration of 0.1 has the highest PF for both water- and PAO-based slurries. For Eq. (30), it is assumed that the microchannel pressure drop dominates the total pressure drop. These results are assumed true for the parameters considered and might change with flow rate, channel dimensions, heat flux, fluid inlet temperature, etc.

V. Conclusions

Thermal performance of EPCM slurry in manifold microchannel heat sinks was studied both experimentally and numerically. The following conclusions can be drawn from the study.

1) Experiments were performed in microchannels of hydraulic diameter 170 μm with water-based slurry and pure water. Flow rates of water and slurry with mass concentration of 0.1 were varied between $5.26 \times 10^{-6}\ \mathrm{m^3/s}$ and $31.54 \times 10^{-6}\ \mathrm{m^3/s}$. Slurry performance was poor compared with pure water for all the flow rates used. This was attributed to the little melting of particles due to their large size (5 μm) and lower thermal conductivity of slurry compared with water.

2) Parametric study was done assuming NEPCM slurry. It was found that thermal conductivity of slurry plays a very important role in the cooling performance of slurry in microchannels, especially in manifold channels that provide flow lengths that are comparable with the developing length of the flow. Results show that the heat transfer coefficient of water-based slurry is lower compared with pure water when the channel hydraulic diameter is 170 μm. For the same configuration, when the base fluid is changed to pure PAO (which has the thermal conductivity equal to that of the PCM), heat transfer coefficient of slurry was higher compared with pure PAO and the heat transfer coefficient increased with increase mass concentrations. Thus, in order to achieve better performance of slurry in developing flows, the presence of PCM particles should enhance the thermal conductivity of the base fluid.

3) Slurry performance also depends on the geometric configuration of the microchannel. Numerical investigation showed that in microchannels of hydraulic diameter of 47 μm, water-based slurry also showed high heat transfer coefficient compared with pure water at all mass concentrations. This is possibly because the flow develops faster in smaller channels.

4) When the same heat transfer coefficient is desired with both slurry and water, results showed that higher mass concentrations are not favorable because of a large pressure drop across the microchannel. Particle mass concentration of 0.1 showed the highest value of performance factor for the parameters considered.

5) Performance of PCM slurries in the case of thermally developing flows depends on many factors. Using a PCM that can enhance the thermal conductivity of slurry, smaller MEPCM particles that can melt instantaneously, narrow channels that can help the flow develop faster, and right inlet temperature can help to achieve maximum benefit of slurry.

Acknowledgments

The authors wish to acknowledge Mark Spector, Program Manager at U.S. Office of Naval Research, for funding this work.

References

[1] Colvin, D. P., and Mulligan, J. C., "Microencapsulated Phase Change for Storage of Heat," NASA George C. Marshall Space Flight Center MFSA-27198, Huntsville, AL, 1987.

[2] Colvin, D. P., and Mulligan, J. C., "Spacecraft Heat Rejection Methods: Active and Passive Heat Transfer for Electronic Systems—Phase I," AFWAL-TR-3074, U.S. Air Force Wright Aeronautical Labs., Dayton, OH, 1986.

[3] Chen, K., and Chen, M. M., "An Analytical and Experimental Investigation of the Convective Heat Transfer of Phase Change Slurry Flows," *Inter. Symposium on Multiphase Flow (2)*, Vol. 2, Ziejiang Univ. Press, Ziejiang, PRC, 1987, pp. 496–501.

[4] Kasza, K. E., and Chen, M. M., "Improvement of the Performance of Solar Energy or Waste Heat Utilization Systems by Using Phase-Change Slurry as an Enhanced Heat Transfer Storage Fluid," *Journal of Solar Energy Engineering*, Vol. 107, No. 3, 1985, pp. 229–236. doi:10.1115/1.3267683

[5] Roy, S. K., and Sengupta, S. K., "An Evaluation of Phase Change Microcapsules for Use in Enhanced Heat Transfer Fluids," *International Communications in Heat and Mass Transfer*, Vol. 18, No. 4, 1991, pp. 495–507. doi:10.1016/0735-1933(91)90064-B

[6] Goel, M., Roy, S. K., and Sengupta, S., "Laminar Forced Convection Heat Transfer in Microcapsulated Phase Change Material Suspension," *International Journal of Heat and Mass Transfer*, Vol. 37, 1994, pp. 593–604. doi:10.1016/0017-9310(94)90131-7

[7] Charunyakorn, P., Sengupta, S., and Roy, S. K., "Forced Convection Heat Transfer in Microencapsulated Phase Change Material Slurry: Flow in Circular Ducts," *International Journal of Heat and Mass Transfer*, Vol. 34, 1991, pp. 819–833. doi:10.1016/0017-9310(91)90128-2

[8] Zhang, Y. W., and Faghri, A., "Analysis of Forced Convection Heat Transfer in Microcapsulated Phase Change Material Suspensions," *Journal of Thermophysics and Heat Transfer*, Vol. 9, No. 4, 1995, pp. 727–732. doi:10.2514/3.731

[9] Yamagishi, Y., Tahkeuchi, H., Pyatenko, A., and Kayukawa, N., "A Technical Evaluation of a Microencapsulated PCM Slurry as a Heat Transfer Fluid," *AIChE Journal*, Vol. 45, No. 4, 1999, pp. 696–707. doi:10.1002/aic.690450405

[10] Alisetti, E. L., and Roy, S. K., "Forced Convection Heat Transfer to Phase Change Material Slurries in Circular Ducts," *Journal of Thermophysics and Heat Transfer*, Vol. 14, 2000, pp. 115–118. doi:10.2514/2.6499

[11] Zhang, Y., Hu, X., and Wang, X., "Theoretical Analysis of Convective Heat Transfer Enhancement of Microencapsulated Phase Change

Material Slurries," *Heat and Mass Transfer*, Vol. 40, 2003, pp. 59–66. doi:10.1007/s00231-003-0410-7

[12] Hao, Y. L., and Tao, Y.-X., "A Numerical Model for Phase-Change Suspension Flow in Microchannels," *Numerical Heat Transfer, Part A, Applications*, Vol. 46, 2004, pp. 55–77. doi:10.1080/10407780490457545

[13] Xing, K. Q., Tao, Y.-X., and Hao, Y. L., "Performance Evaluation of Liquid Flow with PCM Particles in Microchannels," *Journal of Heat Transfer*, Vol. 127, 2005, pp. 931–940. doi:10.1115/1.1929783

[14] Rao, Y., Dammel, F., Stephan, P., and Lin, G., "Convective Heat Transfer Characteristics of Microencapsulated Phase Change Material Suspensions in Minichannels," *Heat and Mass Transfer*, Vol. 44, 2007, pp. 175–186. doi:10.1007/s00231-007-0232-0

[15] Alvarado, J. L., Marsh, C., Sohn, C., Phetteplace, G., and Newell, T., "Thermal Performance of Microencapsulated Phase Change Material Slurry in Turbulent Flow Under Constant Heat Flux," *International Journal of Heat Mass Transfer*, Vol. 50, Nos. 9–10, 2007, pp. 1938–1952. doi:10.1016/j.ijheatmasstransfer.2006.09.026

[16] Kuravi, S., Kota, K. M., Du, J., and Chow, L. C., "Numerical Investigation of Flow and Heat Transfer Performance of Nano-Encapsulated Phase Change Material (NEPCM) Slurry in Microchannels," *Journal of Heat Transfer*, Vol. 131, No. 6, 2009, Paper 062901. doi:10.1115/1.3084123

[17] Sabbah, R., Farid, M. M., and Al-Hallaj, S., "Micro-Channel Heat Sink with Slurry of Water with Micro-Encapsulated Phase Change Material: 3D-Numerical Study," *Applied Thermal Engineering*, Vol. 29, 2009, pp. 445–454. doi:10.1016/j.applthermaleng.2008.03.027

[18] Vand, V., "Theory of Viscosity of Concentrated Suspensions," *Nature*, Vol. 155, 1945, pp. 364–365. doi:10.1038/155364b0

[19] Vand, V., "Viscosity of Solutions and Suspensions," *Journal of Physical and Colloid Chemistry* , Vol. 52, 1948, pp. 300–321. doi:10.1021/j150458a002

[20] Tao, L. C., "Generalized Numerical Solutions of Freezing a Saturated Liquid in Cylinders and Spheres," *AIChE Journal*, Vol. 13, No. 1, 1967, pp. 165–169. doi:10.1002/aic.690130130

[21] Seshadri, V., and Sutera, S. P., "Apparent Viscosity of Coarse, Concentrated Suspensions in Tube Flow," *Transactions of the Society of Rheology*, Vol. 14, No. 3, 1970, pp. 351–373. doi:10.1122/1.549167

[22] COMSOL, Software Package, Ver. 3.4, COMSOL, Inc., Stockholm, Sweden, 1998.

[23] Kreutz, E. W., Pirch, N., Ebert, T., Wester, R., Ollier, B., Loosen, P., and Poprawe, R., "Simulation of Micro-Channel Heat Sinks for Opto-electronic Microsystems," *Microelectronics Journal*, Vol. 31, 2000, pp. 787–790. doi:10.1016/S0026-2692(00)00060-4

[24] Harms, T. M., Kazmierczak, M. J., and Gerner, F. M., "Developing Convective Heat Transfer in Deep Rectangular Microchannels," *International Journal of Heat and Fluid Flow*, Vol. 20, 1999, pp. 149–157. doi:10.1016/S0142-727X(98)10055-3

[25] Karnis, A., Goldsmith, H. L., and Mason, S. G., "The Kinetics of Flowing Dispersions. I. Concentrated Suspensions of Rigid Particles," *Journal of Colloid and Interface Science*, Vol. 22, 1966, pp. 531–553. doi:10.1016/0021-9797(66)90048-8

[26] Watkins, R. W., Robertson, C. R., and Acrivos, A., "Entrance Region Heat Transfer in Flowing Suspensions," *International Journal of Heat and Mass Transfer*, Vol. 19, 1976, pp. 693–695. doi:10.1016/0017-9310(76)90053-3

[27] Wereley, S. T., and Meinhart, C. D., "Micron-Resolution Particle Image Velocimetry," *Micro- and Nano-scale Diagnostic Techniques*, edited by K. S. Breuer, Springer–Verlag, New York, 2005.